Article

Cell Reports

Adipose Fatty Acid Oxidation Is Required for Thermogenesis and Potentiates Oxidative Stress-Induced Inflammation

Graphical Abstract

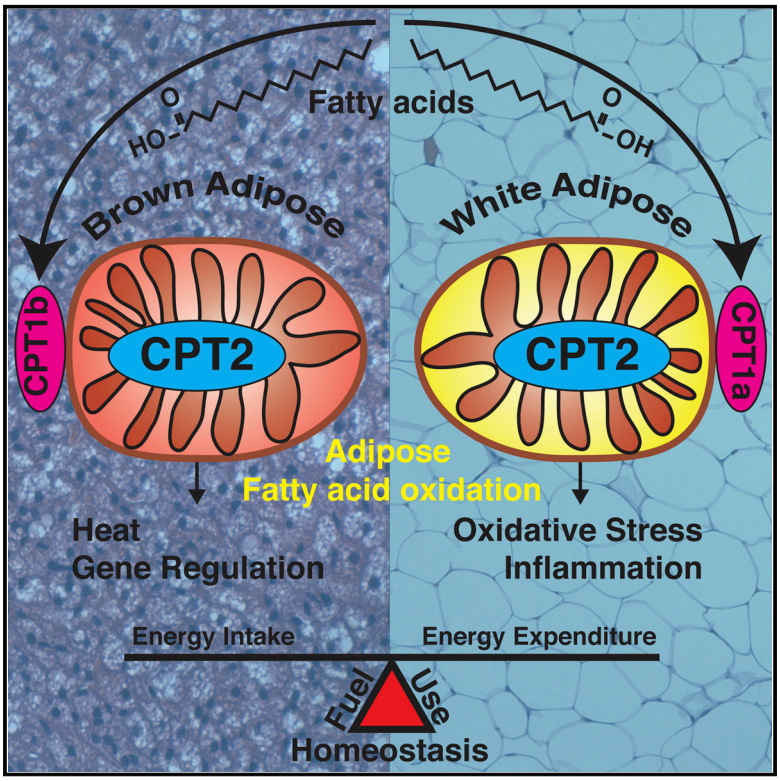

Authors

Jieun Lee, Jessica M. Ellis, Michael J. Wolfgang

Correspondence

mwolfga1@jhmi.edu

In Brief

In order to understand the contribution of adipose tissue fatty acid oxidation to whole-body energy homeostasis, Lee et al. deleted carnitine palmitoyltransferase 2 specifically in adipocytes. They show requirements for adipocyte fatty acid oxidation in cold-induced thermogenesis, gene expression in brown adipocytes, diet-induced adiposity, oxidative stress, and inflammation.

Highlights

- Adipose fatty acid oxidation (FAO) is required for cold-induced thermogenesis
- Adipose FAO is required for agonist-induced thermogenic gene expression
- Loss of adipose FAO does not alter body weight
- Adipose FAO is required for high-fat-induced oxidative stress and inflammation.

Lee et al., 2015, Cell Reports *10*, 266–279
January 13, 2015
http://dx.doi.org/10.1016/j.celrep.2014.12.023

OPEN ACCESS
CellPress

Cell Reports
Article

Adipose Fatty Acid Oxidation Is Required for Thermogenesis and Potentiates Oxidative Stress-Induced Inflammation

Jieun Lee,[1] Jessica M. Ellis,[1,2] and Michael J. Wolfgang[1,*]
[1]Department of Biological Chemistry, Center for Metabolism and Obesity Research, Johns Hopkins University School of Medicine, Baltimore, MD 21205, USA
[2]Present address: Department of Nutrition Science, Purdue University, West Lafayette, IN 47907, USA
*Correspondence: mwolfga1@jhmi.edu
http://dx.doi.org/10.1016/j.celrep.2014.12.023

SUMMARY

To understand the contribution of adipose tissue fatty acid oxidation to whole-body metabolism, we generated mice with an adipose-specific knockout of carnitine palmitoyltransferase 2 ($CPT2^{A-/-}$), an obligate step in mitochondrial long-chain fatty acid oxidation. $CPT2^{A-/-}$ mice became hypothermic after an acute cold challenge, and $CPT2^{A-/-}$ brown adipose tissue (BAT) failed to upregulate thermogenic genes in response to agonist-induced stimulation. The adipose-specific loss of CPT2 resulted in diet-dependent changes in adiposity but did not result in changes in body weight on low- or high-fat diets. Additionally, $CPT2^{A-/-}$ mice had suppressed high-fat diet-induced oxidative stress and inflammation in visceral white adipose tissue (WAT); however, high-fat diet-induced glucose intolerance was not improved. These data show that fatty acid oxidation is required for cold-induced thermogenesis in BAT and high-fat diet-induced oxidative stress and inflammation in WAT.

INTRODUCTION

Ingestion of a calorically dense diet, generally high in fat content, coupled with inactivity leads to increased adiposity and eventual obesity. Obesity in turn is highly correlated with the development of type 2 diabetes, the metabolic syndrome, and cardiovascular disease, among others. The molecular mechanisms by which high-fat diets contribute to these pathologies are not well understood, but several themes have emerged. Implicated in the etiology and progression of obesity-related pathologies is oxidative stress, endoplasmic reticulum stress, and inflammation originating locally at adipose depots but acting systemically to promote insulin resistance (Glass and Olefsky, 2012; Hotamisligil, 2010; Keaney et al., 2003; Kusminski and Scherer, 2012). Reversing or preventing local adipose tissue inflammation may have beneficial systemic effects against insulin resistance. Alternatively, strategies to reverse obesity by increasing adipose energy expenditure have been suggested to improve systemic obesity-related complications (Tseng et al., 2010).

Adult mammals have at least two functionally distinct adipose lineages: unilocular white adipocytes, which function mainly to store fat, and multilocular brown adipocytes, which function mainly to burn fat for thermogenesis. Dysfunctional white adipose tissue (WAT) and brown adipose tissue (BAT) have been implicated in the pathogenesis of obesity and diabetes. BAT is densely packed with mitochondria and requires fatty acid oxidation to fuel heat generation (Ellis et al., 2010; Guerra et al., 1998; Ji et al., 2008; Schuler et al., 2005; Tolwani et al., 2005). Although the oxidation of fatty acids in WAT in the fed state is relatively low, fasting doubles the rate of white adipocyte fatty acid oxidation and is presumably a major fuel in insulin suppressed states (Wang et al., 2003). Changing macronutrient metabolism specifically in adipocytes can lead to changes in adiposity, body weight, and glucose tolerance (Abel et al., 2001; Ahmadian et al., 2011; Lodhi et al., 2012; Vernochet et al., 2012). However, the autonomous contribution of adipose fatty acid oxidation to obesity and insulin resistance remains unknown.

Mitochondrial long-chain fatty acid β-oxidation requires successive carnitine acyltransferases to translocate acyl-coenzyme As (acyl-CoAs) from the cytoplasm into the mitochondrial matrix (Wolfgang and Lane, 2006). The initial and rate-setting enzyme, CPT1, generates acylcarnitines that can traverse the mitochondrial membranes via specific transporters. CPT1 is allosterically inhibited by the rate-determining metabolite in de novo fatty acid synthesis, malonyl-CoA; therefore, the balance of fatty acid synthesis and oxidation is metabolically coordinated posttranslationally. Once inside the mitochondrial matrix, CPT2 generates acyl-CoAs from acylcarnitines to initiate the β-oxidation of long-chain fatty acids to acetyl-CoA. Fatty acids contain an abundant energy potential, making them ideal for storage during energy surplus and mobilization during energy deficits. Fatty acid oxidation efficiently generates energy but can also promote the generation of reactive oxygen species (ROS). ROS can potentiate oxidative stress and inflammation, which can impair insulin sensitivity (Houstis et al., 2006).

Although it is clear that fatty acid oxidation is a critical and fundamental metabolic endpoint in humans (Longo et al., 2006) and rodents (Ji et al., 2008; Nyman et al., 2005), it is not clear

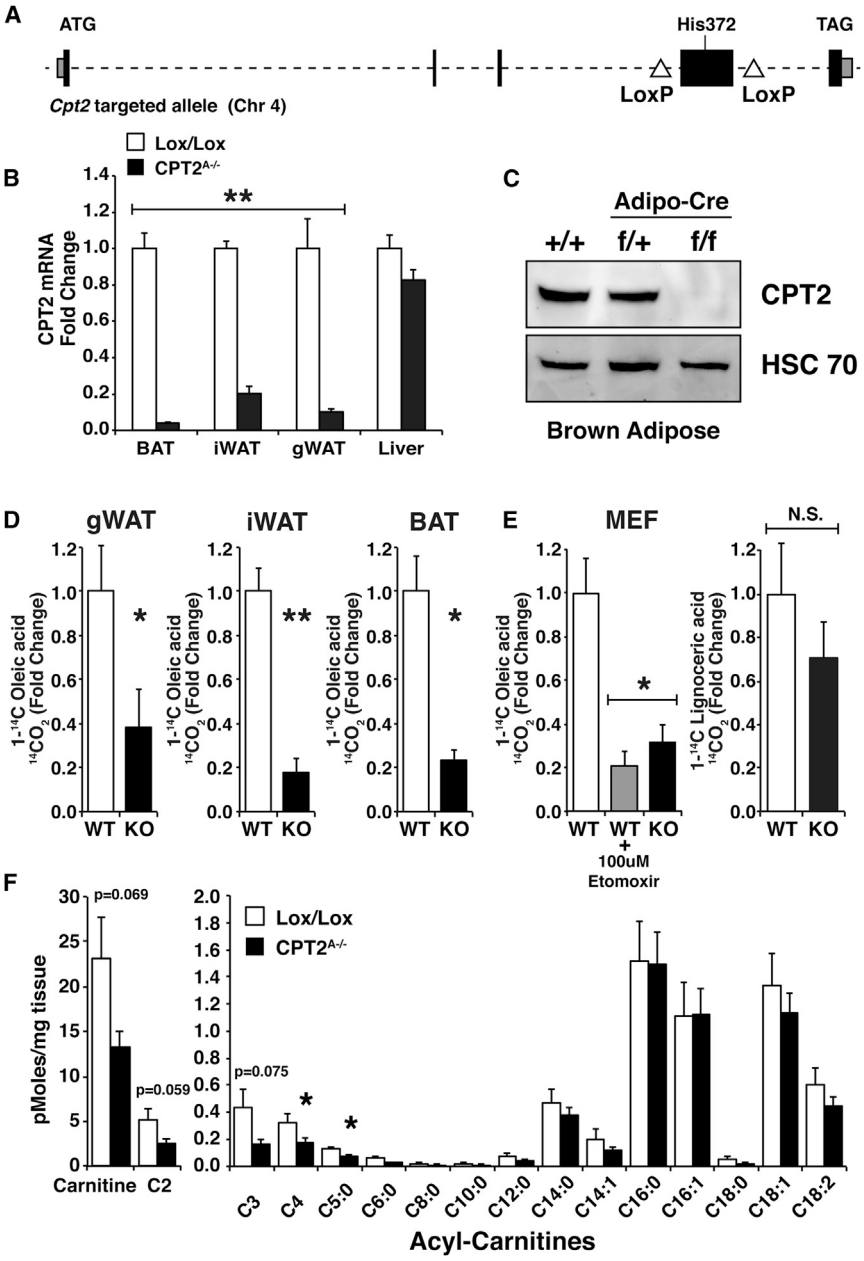

Figure 1. Generation of Mice with an Adipose-Specific KO of CPT2

(A) Gene targeting strategy for the *Cpt2* gene. Triangles represent *loxP* sites.

(B) mRNA for *Cpt2* in adipose depots and liver of control and $CPT2^{A-/-}$ mice (n = 8).

(C) Western blot for CPT2 in BAT of control, $CPT2^{A-/+}$, and $CPT2^{A-/-}$ mice.

(D) Oxidation of 1-^{14}C-oleic acid to $^{14}CO_2$ in control and $CPT2^{A-/-}$ adipose depot explants (n = 5).

(E) Oxidation of 1-^{14}C-oleic acid or 1-^{14}C-lignoceric acid to $^{14}CO_2$ in control and CPT2 KO MEFs (n = 5).

(F) Acylcarnitine profile of iWAT in control and $CPT2^{A-/-}$ mice (n = 8).

Data are expressed as mean ± SEM. *p < 0.05; **p < 0.001; N.S., not significant. Open bars represent control, and black bars represent loss of CPT2.

RESULTS

Generation of Mice with an Adipose Tissue-Specific Deletion of CPT2

Mitochondrial long-chain fatty acid oxidation requires sequential carnitine acyltransferases to translocate acyl-CoAs into the mitochondrial matrix. The regulated and rate setting enzyme, CPT1, is encoded by multiple isoenzymes that can functionally compensate in some tissues (Haynie et al., 2014). Therefore, to generate a mouse model to assess the tissue-specific roles and requirements of fatty acid oxidation, we generated a conditional loss-of-function allele for CPT2, an enzyme required in mitochondrial long-chain fatty acid β-oxidation that is encoded by a single gene. C57BL/6 embryonic stem cells were used to target *loxP* recombination sites surrounding exon 4 of the *Cpt2* gene (Figure 1A). Exon 4 encompasses approximately one-third of the protein coding sequence including all of the critical catalytic residues (Hsiao et al., 2006). Loss of exon 4 is predicted to additionally cause a frameshift in the remaining exons. To produce mice with a loss of CPT2 specifically in adipocytes, we bred $CPT2^{lox/lox}$ mice to adipocyte specific adiponectin-Cre transgenic mice (Eguchi et al., 2011). The resulting adipose-specific CPT2 knockout (KO) mice, $CPT2^{A-/-}$, have a loss of *Cpt2* mRNA in all adipose depots examined (Figure 1B). Furthermore, CPT2 protein is substantially reduced in BAT of $CPT2^{A-/-}$ mice (Figure 1C). As expected, ex vivo gonadal WAT (gWAT), inguinal WAT (iWAT), and BAT explants derived from $CPT2^{A-/-}$ mice had a greatly suppressed ability to oxidize radiolabeled 1-^{14}C-oleic acid (Figure 1D). Long chain mitochondrial fatty acid β-oxidation cannot proceed in the absence of CPT2. The remaining oxidation

how adipocyte fatty acid oxidation affects whole-body metabolism in an autonomous manner. Therefore, we generated a conditional loss-of-function allele for CPT2, an obligate step in mitochondrial long-chain fatty acid β-oxidation that is encoded by a single gene. Here we show that adipose tissue fatty acid oxidation is required not only for acute cold adaptation but also for the induction of thermogenic genes in BAT. The loss of adipose fatty acid oxidation altered adiposity in a diet-dependent manner but did not lead to diet-induced changes in body weight. Furthermore, we show that in WAT, the loss of fatty acid oxidation reduces high-fat-induced oxidative stress and inflammation but does not alter the progression of obesity or glucose intolerance.

of oleic acid in tissues was presumably due to either peroxisomal fatty acid oxidation or oxidation in nonparenchymal cells within the adipose depots. To test this directly, we derived and immortalized mouse embryonic fibroblasts (MEFs) from $CPT2^{lox/lox}$ embryos and infected them with a control or Cre recombinase expressing virus. The oxidation of 1-^{14}C-oleic acid in $CPT2^{lox/lox}$ MEFs was severely blunted by incubating cells with a large dose (100 μM) of the mitochondrial fatty acid oxidation inhibitor etomoxir. The genetic loss of CPT2 in MEFs suppressed oleic acid oxidation to the same degree as etomoxir (Figure 1E). However, the oxidation of the very long chain lignoceric acid (C24:0), which is oxidized mainly in peroxisomes, was not significantly changed (Figure 1E). Therefore, the deletion of CPT2 represents an effective strategy for inhibiting long chain mitochondrial fatty acid β-oxidation.

To determine how the loss of CPT2 alters white adipose fatty acid oxidative metabolites, we measured the steady-state concentration of carnitine and acyl-carnitine species in iWAT of control and $CPT2^{A-/-}$ mice. Although CPT2 deficiency results in the inability to utilize long chain acyl-carnitines and people with CPT2 mutations are diagnosed by the elevation of these metabolites in serum, $CPT2^{A-/-}$ mice did not have increased long chain acyl-carnitine species in iWAT. Instead, $CPT2^{A-/-}$ iWAT had a strong trend toward suppressed free carnitine and acetyl-carnitine and statistically significant reductions in several short chain acyl-carnitines (Figure 1F). We conclude that long chain acyl-carnitines do not build up in WAT but are readily transported out of the adipocyte resulting in a tissue specific carnitine deficiency due to the inability to properly recycle carnitine in $CPT2^{A-/-}$ WAT. In summary, we have generated mice with an adipose-specific defect in mitochondrial long-chain fatty acid oxidation that is mediated by the loss of an obligate noncompensatory step in fatty acid oxidation.

Adipose Fatty Acid Oxidation Is Required for Cold-Induced Thermogenesis

BAT is essential for heat generation during an acute cold exposure in perinatal and adult mammals (Kozak, 2010; Lowell et al., 1993; Tseng et al., 2010). The requirement of fatty acid oxidation during cold thermogenesis is made evident by cold-intolerant phenotypes of whole-body KO mouse models of the acyl-CoA dehydrogenase enzymes (Guerra et al., 1998; Schuler et al., 2005; Tolwani et al., 2005). To determine the autonomous requirement of adipose fatty acid oxidation during adaptive thermogenesis, we placed 12-week-old control and $CPT2^{A-/-}$ female mice at 4°C and measured their body temperature over 3 hr. Although all of the mice visibly shivered, cold intolerance was evident in $CPT2^{A-/-}$ mice, reaching critical hypothermia (30°C) within 3 hr (Figure 2A). The body weights of 12-week-old female $CPT2^{A-/-}$ mice were not different (Figure 2B). Upon dissection, $CPT2^{A-/-}$ interscapular BAT was visibly lipid laden, displaying a milky appearance in contrast to the dark brown color of control BAT (Figure 2C). Histologic evaluation demonstrated increased lipid droplet accumulation that did not dissipate upon cold stimulation (Figure 2D). Consistent with these morphologic changes, cold-exposed $CPT2^{A-/-}$ BAT maintained ~3-fold increase in triglyceride content compared to BAT from control mice (Figure 2E). Evaluation of serum metabolites showed normal responses of serum glucose, ketone bodies, and triglycerides to cold stimulation in $CPT2^{A-/-}$ mice. However, compared to controls, $CPT2^{A-/-}$ mice had increased serum free fatty acids and decreased glycerol during cold stimulation, likely due to their inability to utilize the mobilized fatty acids in CPT2 null BAT (Figure 2F). These data show that adipose fatty acid oxidation is required for acute cold-induced thermogenesis.

BAT Fatty Acid Oxidation Is Required for Agonist-Induced Thermogenic Gene Expression

To understand the transcriptional control of BAT metabolism in $CPT2^{A-/-}$ mice, we determined the expression of fatty acid catabolic and anabolic genes. After a 3 hr cold stimulation, the fatty acid oxidative genes *Acox1*, *Cpt1b*, and *Lcad* were suppressed in $CPT2^{A-/-}$ BAT (Figure 3A). Malonyl-CoA decarboxylase (*Mlycd*), which decarboxylates malonyl-CoA and therefore disinhibits CPT1, was greatly suppressed in both basal and cold-stimulated $CPT2^{A-/-}$ BAT. Additionally, fatty acid biosynthetic genes *Pcx*, *Acaca*, and *Elovl6* were suppressed after a 3 hr cold stimulation in $CPT2^{A-/-}$ BAT compared to controls (Figure S1A). These data suggest that the loss of fatty acid oxidation in BAT feeds back to inhibit genes in fatty acid oxidation. To better understand the role of fatty acid oxidation on thermogenic programing in BAT, we measured the transcriptional response of BAT to cold stimulation. The canonical cold-induced genes *Ucp1*, *Pgc1α*, and *Dio2* were induced robustly in BAT of control mice after 3 hr at 4°C but were unresponsive in $CPT2^{A-/-}$ BAT (Figure 3B). In fact, *Ucp1* and *Dio2* were suppressed constitutively even at room temperature. *Ucp1* and *Pgc1a* are thermogenic genes regulated by adrenergic signaling upon cold exposure. Therefore, we determined if $CPT2^{A-/-}$ BAT was responsive to adrenergic stimulation by injecting $CPT2^{A-/-}$ and control mice with the selective β3-adrenergic agonist CL-316243 (10 mg/kg) and collected BAT 3 hr later. Unlike the control, $CPT2^{A-/-}$ BAT elicited no increase in the mRNA abundance of *Ucp1* or *Pgc1α* (Figure 3B). This suggests a strong defect in $CPT2^{A-/-}$ BAT thermogenic gene expression.

To determine where in the adrenergic signaling pathway $CPT2^{A-/-}$ BAT was impaired, we collected control and $CPT2^{A-/-}$ BAT explants and stimulated them ex vivo with 10 μM CL-316243, the β-adrenergic agonist isoproterenol, or the adenylyl cyclase activator forskolin, in the presence of 200 μM fatty acids (2:1 oleate:palmitate). All of these activators robustly induced *Ucp1* in control explants; however, $CPT2^{A-/-}$ BAT was unable to induce *Ucp1* (Figure 3C). These data suggest that the defect in cold-induced thermogenic gene expression is mediated downstream of the adrenergic receptor.

To determine if $CPT2^{A-/-}$ BAT was activating signaling downstream of adrenergic stimulation, we probed for protein kinase A (PKA) targets of adrenergic signaling after a 30 min stimulation with 10 mg/kg CL-316243 in vivo. Utilizing a PKA phosphorylated substrate specific antibody, both control and $CPT2^{A-/-}$ BAT showed robust CL-316243 mediated phosphorylation (Figure 3D). Additionally, cAMP response element-binding protein (CREB) phosphorylation, the canonical transcription factor downstream of adrenergic stimulation, elicited a robust phosphorylation in both control and $CPT2^{A-/-}$ BAT (Figure 3E). These

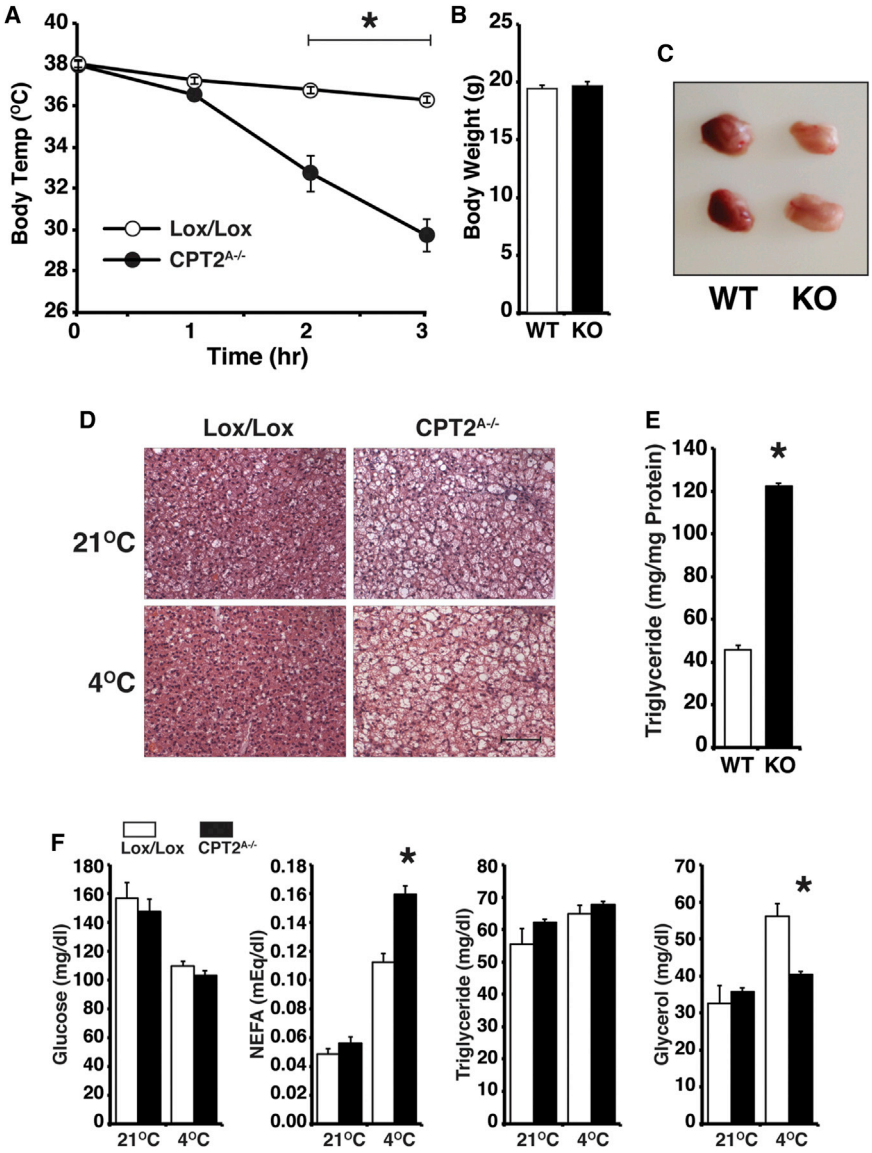

Figure 2. Adipose Fatty Acid Oxidation Is Required for Acute Cold-Induced Thermogenesis

(A) Body temperature of control and CPT2$^{A-/-}$ mice subjected to a 3 hr cold challenge (n = 10–13).

(B) Body weights of 12-week-old female control and CPT2$^{A-/-}$ mice (n = 22-26).

(C) Gross morphology of control and CPT2$^{A-/-}$ BAT after 2 hr of cold exposure.

(D) Hematoxylin and eosin (H&E)-stained sections of BAT from control and CPT2$^{A-/-}$ mice at 21°C and 3 hr at 4°C. Scale bar is 100 μM.

(E) Triglyceride content of BAT of control and CPT2$^{A-/-}$ mice after 3 hr at 4°C (n = 5).

(F) Serum metabolites in control and CPT2$^{A-/-}$ mice at 21°C and 3 hr at 4°C (n = 8).

Data are expressed as mean ± SEM. *p < 0.001. Open bars represent control and black bars represent loss of CPT2.

data show that CPT2$^{A-/-}$ BAT can activate adrenergic signaling and phosphorylation of downstream targets such as CREB. This suggests the defect in agonist-induced thermogenic gene expression is likely at the level of transcriptional regulation. Taken together, these experiments show that CPT2$^{A-/-}$ BAT is resistant to agonist-induced thermogenic gene expression and further suggest that fatty acid oxidation in BAT is coupled to agonist-induced transcription.

CPT2$^{A-/-}$ Mice Are Defective in Environmental Temperature Adaptation

Mammals can dramatically alter their physiology to adapt to the ambient temperature. Cold acclimation of UCP1KO mice is sufficient to rescue their acute cold intolerance (Golozoubova et al., 2001; Ukropec et al., 2006). To test the role of adipose fatty acid oxidation on this adaptation, we cold acclimatized CPT2$^{A-/-}$ mice to 15°C and then subjected them to an acute 4°C cold challenge. At 15°C, CPT2$^{A-/-}$ and control mice had lower body temperatures (~35.5°C) that upon cold challenge initially rose rapidly. However, CPT2$^{A-/-}$ mice could not maintain body temperature and after 4 hr reached critical hypothermia (Figure 3F). Again, *Ucp1* and *Dio2* mRNA abundance was suppressed in CPT2$^{A-/-}$ BAT (Figure 3G). This suggests that adipose fatty acid oxidation has additional roles other than merely activating UCP1 in BAT. Next, we asked if the inhibition of agonist-induced thermogenic gene expression at 21°C and 15°C was due to tonic activation of thermogenic signaling and therefore constitutively inhibited via negative feedback. To eliminate tonic basal thermogenic signaling, we acclimatized CPT2$^{A-/-}$ and control mice to a thermoneutral environment (30°C). We then injected the mice with 10 mg/kg CL-316243 or vehicle and collected BAT 3 hr later. Thermoneutral acclimatization did not improve agonist-induced thermogenic gene expression in CPT2$^{A-/-}$ mice. In fact, the difference between control and CPT2$^{A-/-}$ mice was further exacerbated, suggesting that the transcriptional defect is not due to tonic inhibition but is a primary defect (Figure 3H). These data show that adipose fatty acid oxidation is critical for thermal adaptation.

Loss of Adipose Fatty Acid Oxidation Disrupts Mitochondrial Homeostasis in BAT

The lack of agonist-induced *Pgc1α* expression, a gene key to mitochondrial biogenesis, prompted us to examine mitochondrial proteins and mitochondrial density in CPT2$^{A-/-}$ BAT. Several mitochondrial proteins were suppressed in CPT2$^{A-/-}$ BAT under basal (21°C) conditions, including ACO2 and MCAD (Figures 3I and S1). These changes were exacerbated

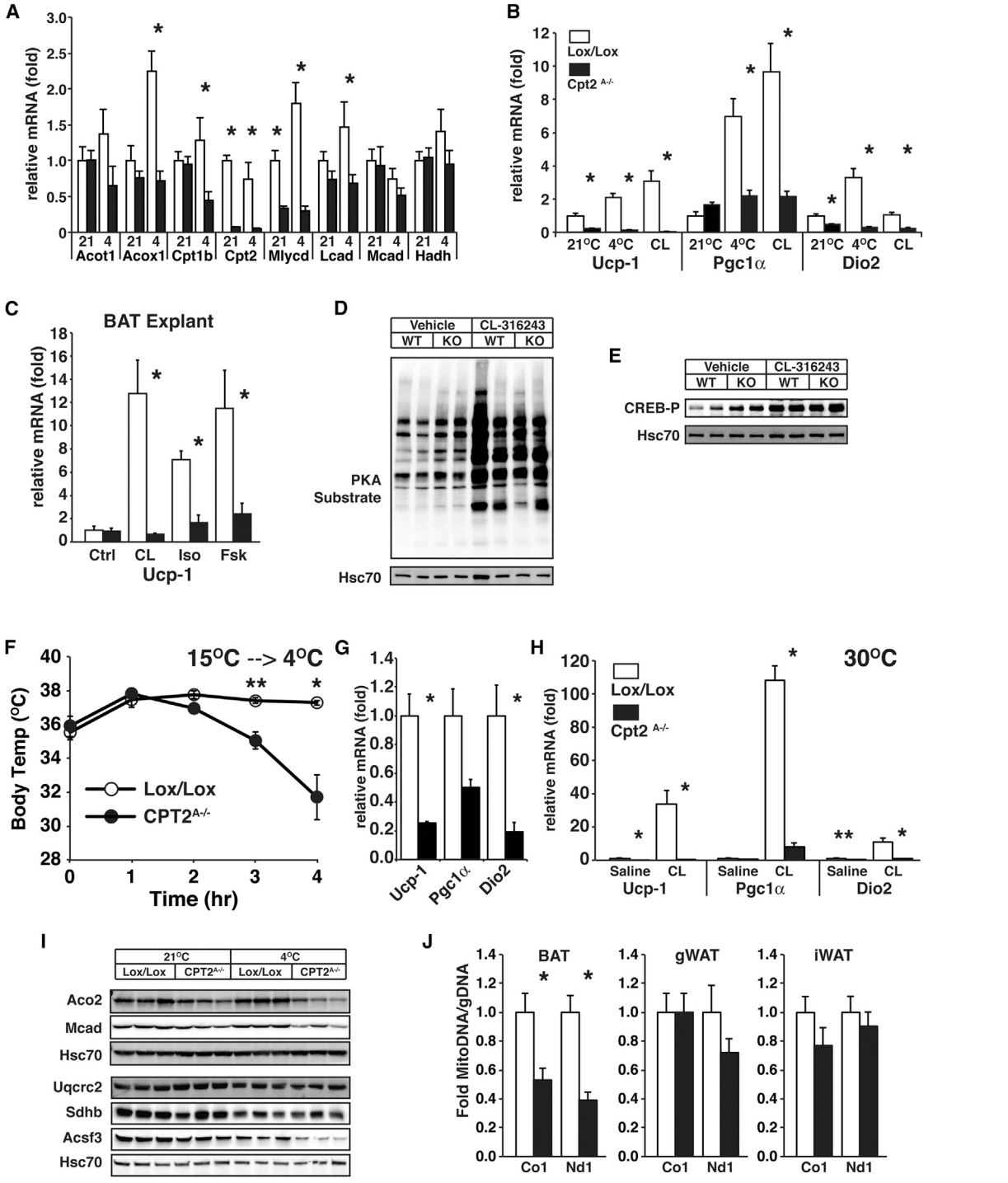

Figure 3. Adipose Fatty Acid Oxidation Is Required for Agonist-Induced Thermogenic Gene Expression and Mitochondrial Homeostasis

(A) mRNA expression of fatty acid oxidative genes in BAT of control and CPT2$^{A-/-}$ mice at 21°C or after 3 hr at 4°C (n = 8).

(B) mRNA expression of *Ucp1*, *Pgc1α*, and *Dio2* in BAT of control and CPT2$^{A-/-}$ mice at 21°C (n = 8), after 3 hr at 4°C (n = 8), or 3 hr after injection with 10 mg/kg CL-316243 (n = 5).

(C) mRNA expression of *Ucp1* in BAT explants treated with 10 μM CL-316243, isoproterenol, or forskolin (n = 5).

(D) Western blot for PKA phosphorylated substrates in BAT of control and CPT2$^{A-/-}$ mice treated with 10 mg/kg CL-316243 for 30 min in vivo.

(E) Western blot for P-CREB (Ser-133) in BAT of control and CPT2$^{A-/-}$ mice treated with 10 mg/kg CL-316243 for 30 min in vivo.

(F) Body temperature of control and CPT2$^{A-/-}$ mice acclimatized to 15°C and subjected to a 4 hr cold challenge at 4°C (n = 5).

(G) mRNA expression of *Ucp1*, *Pgc1α*, and *Dio2* in BAT of 15°C acclimatized control and CPT2$^{A-/-}$ mice after a 4 hr cold challenge (n = 5).

(legend continued on next page)

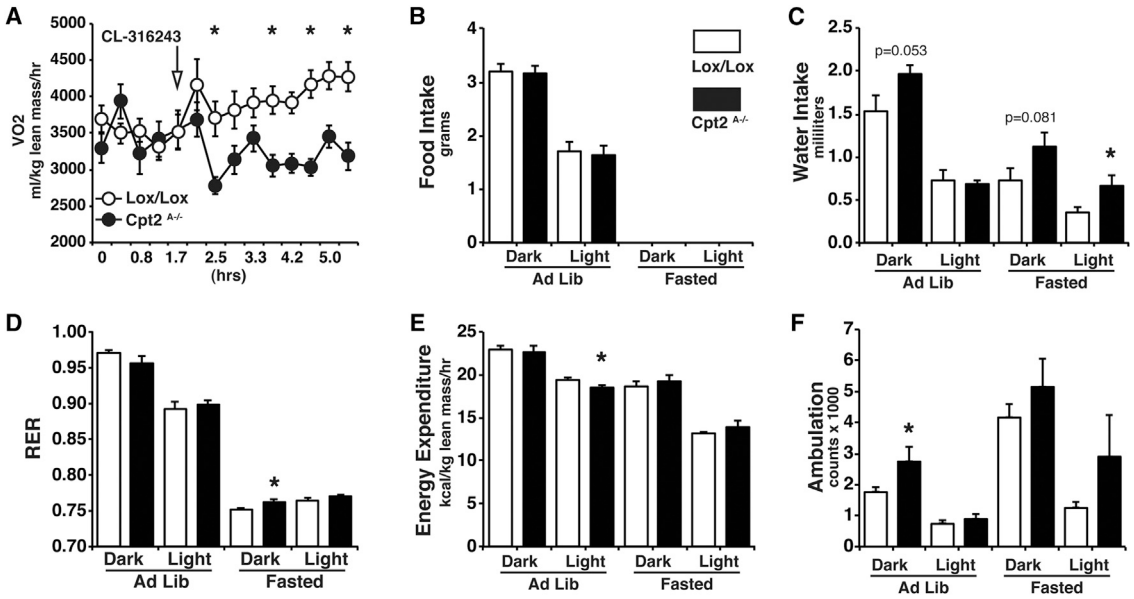

Figure 4. Contribution of Adipose Fatty Acid Oxidation to Energy Expenditure

(A) VO2 consumption of control and CPT2$^{A-/-}$ male mice treated with 10 mg/kg CL-316243.

(B) Food intake of control and CPT2$^{A-/-}$ mice.

(C) Water intake of control and CPT2$^{A-/-}$ mice under ad libitum and fasting under dark and light cycles.

(D) Respiratory exchange ratio of control and CPT2$^{A-/-}$ mice under ad libitum and fasting under dark and light cycles.

(E) Energy expenditure of control and CPT2$^{A-/-}$ mice under ad libitum and fasting under dark and light cycles.

(F) Ambulation rates of control and CPT2$^{A-/-}$ mice under ad libitum and fasting under dark and light cycles (n = 10–14).

Data are expressed as means ± SEM. *p < 0.05. Open bars represent control, and black bars represent loss of CPT2.

after 3 hr of cold stimulation. To determine mitochondrial number, we quantified BAT mitochondrial DNA and found that gWAT and iWAT maintained normal mitochondrial DNA content whereas CPT2$^{A-/-}$ BAT had about a 2-fold suppression in mitochondrial DNA (Figure 3J). These data show that mitochondrial long-chain fatty acid oxidation in BAT is important not only for cellular bioenergetics but also for nuclear-encoded mitochondrial gene expression, mitochondrial protein abundance, and density.

Bioenergetic Contribution of Adipose Fatty Acid Oxidation

In the absence of cold stimulation, it was not clear what the contribution of adipose fatty acid oxidation is to whole-body energy expenditure under standard physiological conditions or perturbations. To determine the physiological contributions of adipose fatty acid oxidation, we housed control and CPT2$^{A-/-}$ mice individually in metabolic cages and measured metabolic parameters continuously during ad libitum feeding and fasting conditions. Consistent with a requirement for fatty acid oxidation during cold exposure, an injection of CL-316243 rapidly increased oxygen consumption in control mice but was completely ineffective in altering oxygen consumption in CPT2$^{A-/-}$ mice (Figure 4A). Unlike other models where changes in fatty oxidation drive changes in feeding behavior (Abu-Elheiga et al., 2001), CPT2$^{A-/-}$ mice had no changes in food intake compared to control mice (Figure 4B). Interestingly, CPT2$^{A-/-}$ mice consumed more water than controls during the course of the experiment, particularly during fasting (Figure 4C). This suggests that adipose tissue fatty acid oxidation may play a role in the generation and balance of water, similar to the role of lipid oxidation during hibernation (Nelson et al., 1973). There were minor reductions in energy expenditure and increased respiratory exchange ratio in CPT2$^{A-/-}$ mice relative to controls (Figures 4D and 4E). Additionally, there was a modest increase in ambulatory activity in CPT2$^{A-/-}$ mice that may reflect a compensatory requirement of energy expenditure from skeletal muscle (Figure 4F). These data show that adipose fatty acid oxidation contributes to overall energy expenditure in the absence of cold stimulation, albeit minimally.

Loss of Adipose Fatty Acid Oxidation Results in Diet-Dependent Changes in Adiposity, but Not Body Weight

It has been suggested that mitochondrial dysfunction and suppressed BAT or WAT fatty acid oxidation contributes to changes in body weight and glucose tolerance (Keaney et al.,

(H) mRNA expression of *Ucp1*, *Pgc1α*, and *Dio2* in BAT of control and CPT2$^{A-/-}$ mice acclimatized to 30°C and injected with vehicle or 10 mg/kg CL-316243 for 3 hr (n = 4–5).

(I) Western blot of mitochondrial proteins in BAT of control and CPT2$^{A-/-}$ mice at 21°C or after 3 hr at 4°C.

(J) Mitochondrial DNA content of BAT and gWAT from control and CPT2$^{A-/-}$ mice (n = 10–12).

Data are expressed as mean ± SEM. *p < 0.01; **p < 0.05. Open bars represent control, and black bars represent loss of CPT2.

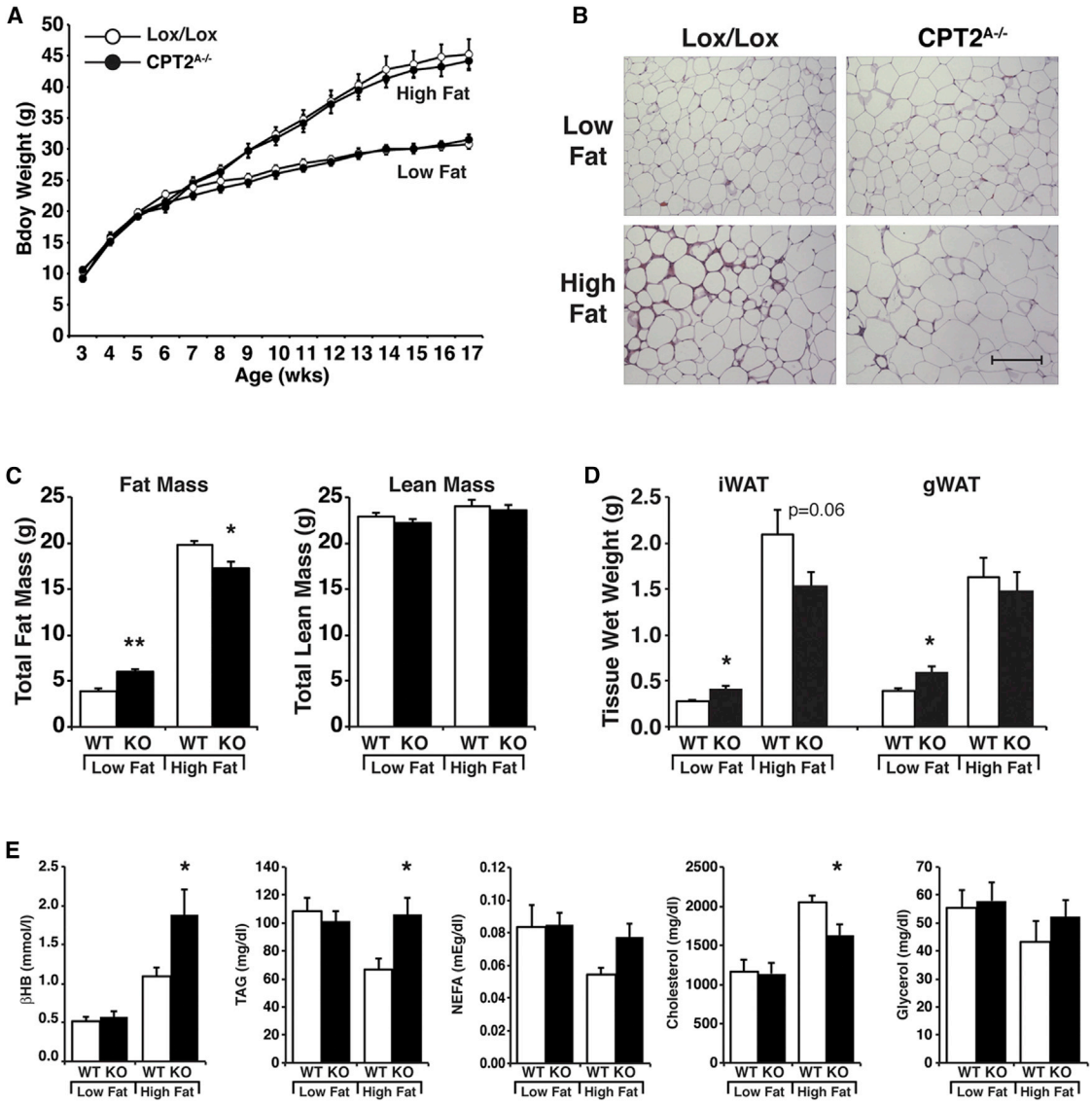

Figure 5. The Loss of Adipose Fatty Acid Oxidation Affects Diet-Dependent Adiposity, but Not Body Weight

(A) Body weights of control and CPT2$^{A-/-}$ male mice fed a low or high fat diet (n = 13–18).

(B) H&E-stained sections of gWAT from control and CPT2$^{A-/-}$ mice fed low- or high-fat diets. Scale bar is 250 μM.

(C) Body compositions measured by EchoMRI for control and CPT2$^{A-/-}$ mice fed low- or high-fat diets (n = 13–18).

(D) Wet weights of iWAT and gWAT unilateral depots for control and CPT2$^{A-/-}$ mice fed low- or high-fat diets (n = 13–18).

(E) Serum metabolites in control and CPT2$^{A-/-}$ mice fed low- or high-fat diets (n = 8).

Data are expressed as means ± SEM. **p < 0.01; *p < 0.05. Open bars represent control, and black bars represent loss of CPT2.

2003; Kusminski and Scherer, 2012). CPT2$^{A-/-}$ BAT is both bioenergetically and transcriptionally unable to support thermogenesis. Additionally, we have shown that the oxidation of fatty acids in adipose tissue is not a major determinant of whole-animal bioenergetics during ad libitum or fasting conditions. To determine the consequences of a chronic long-term inability to oxidize fatty acids in adipocytes on body weight, we placed control and CPT2$^{A-/-}$ mice on matched low- and high-fat diets for 12 weeks and measured their body weights weekly. CPT2$^{A-/-}$ mice elicited no change in body weight, compared to control littermates, fed either a high-fat or low-fat diet (Figure 5A). Evaluation of fat and lean content revealed a 64% increase in fat mass in low-fat-fed CPT2$^{A-/-}$ mice (Figures 5B and 5C). Measurement of fat pad weights of low-fat-fed CPT2$^{A-/-}$ mice showed 67% increases in both gonadal and inguinal fat pads (Figure 5D). High-fat-fed CPT2$^{A-/-}$ mice displayed a suppression of fat mass that was mainly the result of changes in inguinal adiposity (Figures 5C and 5D). These seemingly paradoxical results are actually consistent with other models with dysfunctional adipose fatty acid oxidation or uncoupling (Ellis et al., 2010; Liu et al., 2003) and likely reflect compensatory increases in energy expenditure in tissues other than adipose. The expression of

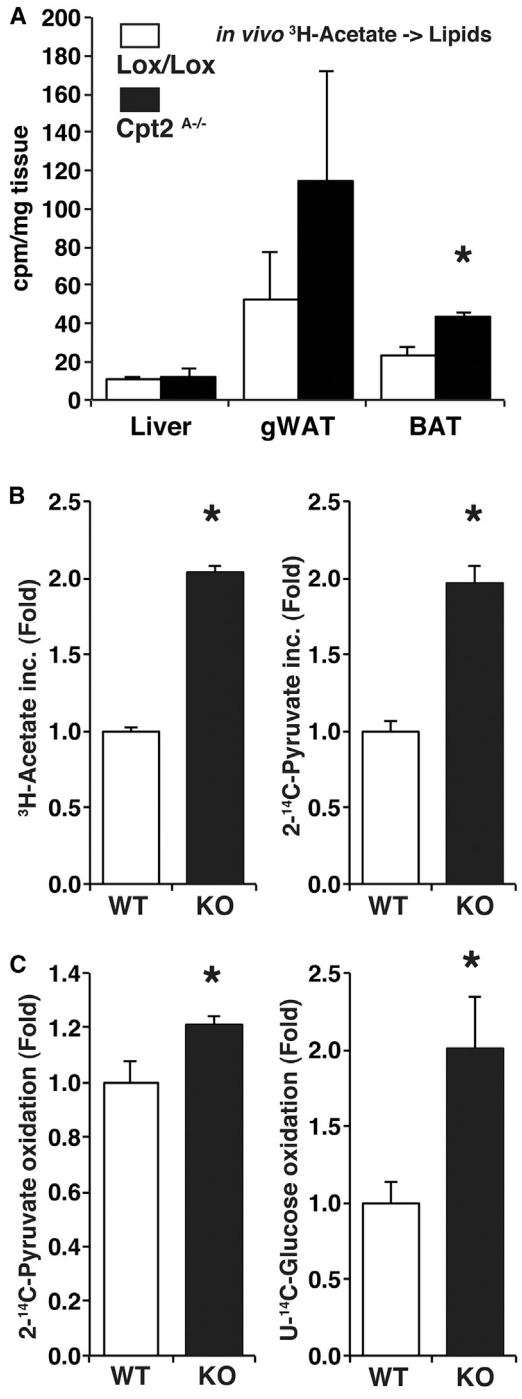

Figure 6. The Loss of Fatty Acid Oxidation Alters Carbohydrate Metabolic Flux

(A) De novo lipogenesis of control and CPT2$^{A-/-}$ liver, gWAT, and BAT from a 1 hr injection of ^{3}H-acetate normalized to tissue wet weight (n = 4–5).

(B) De novo lipogenesis of control and CPT2$^{A-/-}$ MEFs from ^{3}H-acetate or 2-^{14}C-pyruvate normalized to protein concentration (n = 6).

(C) Substrate oxidation of control and CPT2$^{A-/-}$ MEFs from 2-^{14}C-pyruvate or U-^{14}C-glucose normalized to protein concentration (n = 5).

Data are expressed as mean ± SEM. *p < 0.05. Open bars represent control, and black bars represent loss of CPT2.

fatty acid biosynthetic genes was largely unchanged between control and CPT2$^{A-/-}$ gWAT; however, there were increases in fatty acid oxidative genes *Cpt1a* and *Mlycd* in low-fat-fed CPT2$^{A-/-}$ gWAT (Figure S2A). This suggests distinct regulatory mechanisms in CPT2$^{A-/-}$ BAT and gWAT, since *Cpt1b* and *Mlycd* were decreased in CPT2$^{A-/-}$ BAT. Consistent with increased compensatory energy expenditure, high-fat-fed CPT2$^{A-/-}$ mice displayed about a 2-fold increase in circulating ketones compared to control high-fat-fed mice (Figure 5E). Analysis of gene expression in iWAT and liver of control and CPT2$^{A-/-}$ mice shows that under high-fat conditions, many of the changes between the genotypes were concentrated in the iWAT (Figure S2B). Conversely, liver from control and CPT2$^{A-/-}$ mice showed most differences after low-fat feeding (Figure S2C). This shows that individual tissues and even different adipose depots respond disparately. These data demonstrate that the loss of adipose fatty acid oxidation does not contribute to changes in total body weight regardless of dietary lipid content, but that CPT2$^{A-/-}$ mice displayed differences in adiposity that were diet dependent.

Loss of Adipose Fatty Acid Oxidation Is Compensated in Part by Altered Carbohydrate Metabolism

The diet-dependent changes in adiposity in CPT2$^{A-/-}$ mice are consistent with other cold-intolerant models (Ellis et al., 2010; Liu et al., 2003). Nonetheless, we were interested in determining the flux of macronutrients in tissues lacking CPT2. First, we directly tested the ability of CPT2$^{A-/-}$ mice to fully oxidize radiolabeled 1-^{14}C oleic acid in vivo. Consistent with the indirect calorimetry data, we did not observe differences in whole-body fatty acid oxidation between control and CPT2$^{A-/-}$ mice (Figure S3). Next, we determined the rate of de novo fatty acid synthesis by injecting ^{3}H-acetate to control and CPT2$^{A-/-}$ mice for 3 hr and extracting lipids from liver, gWAT, and BAT. Although the livers of control and CPT2$^{A-/-}$ mice had equal incorporation of ^{3}H-acetate into lipids, both gWAT and BAT had an ~2-fold increase in incorporation (Figure 6A). This suggested that there was an increase in carbohydrate utilization in cells where CPT2 was deleted. Therefore, we assayed ^{3}H-acetate incorporation into lipids in control and CPT2KO MEFs. Consistent with the in vivo data, CPT2KO MEFs had a 2-fold increase in de novo lipogenesis from both ^{3}H-acetate and 2-^{14}C-pyruvate (Figure 6B). Additionally, we examined the oxidation of radiolabeled 2-^{14}C-pyruvate and U-^{14}C-glucose to $^{14}CO_2$. While pyruvate oxidation was increased ~20%, glucose oxidation was increased 2-fold over control cells (Figure 6C). These data show that the loss of fatty acid oxidation is compensated in part by increased carbohydrate flux.

Adipose Fatty Acid Oxidation Potentiates High-Fat Diet-Induced Oxidative Stress and Inflammation

The oxidation of fatty acids generates a substantial oxidative burden. It has been previously demonstrated that high-fat feeding increases oxidative stress and damaging oxidative end products particularly within gWAT (Furukawa et al., 2004). Given the role of fatty acid oxidation in the generation of ROS, we profiled genes known to be involved in oxidative stress in high-fat-fed control and CPT2$^{A-/-}$ gWAT by quantitative PCR (qPCR)

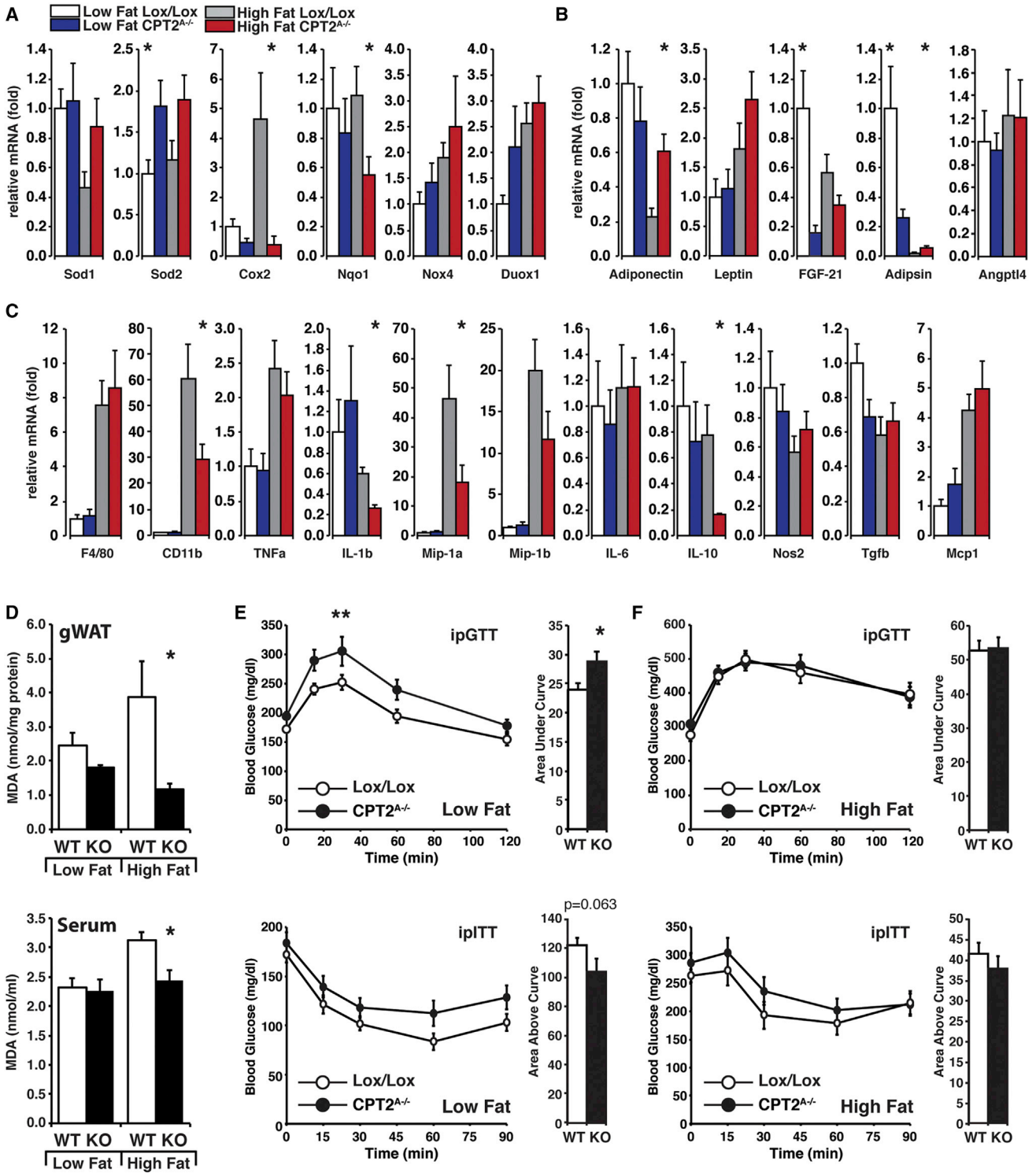

Figure 7. Adipose Fatty Acid Oxidation Potentiates High-Fat-Induced Oxidative Stress and Inflammation

(A) Quantitative RT-PCR (qRT-PCR) of oxidative stress genes from gWAT of control and CPT2$^{A-/-}$ mice fed a low- or high-fat diet (n = 8).

(B) qRT-PCR of adipokines from gWAT of control and CPT2$^{A-/-}$ mice fed a low- or high-fat diet (n = 8).

(C) qRT-PCR of inflammatory genes from gWAT of control and CPT2$^{A-/-}$ mice fed a low- or high-fat diet (n = 8).

(D) TBARS assay from gWAT and serum of control and CPT2$^{A-/-}$ mice fed a low- or high-fat diet (n = 5).

(legend continued on next page)

array. Multiple genes involved in detoxifying ROS were increased and several more involved in generating ROS were suppressed (Figure S4). To confirm and extend this data, we analyzed the genes and pathways identified in the qPCR screen in gWAT RNA isolated from both low- and high-fat-fed control and CPT2$^{A-/-}$ mice. *Sod1* and *Sod2* trended toward an increase under high-fat conditions, and *Sod2* was significantly increased ~2-fold in low-fat-fed CPT2$^{A-/-}$ gWAT. Genes that increase oxidative stress were suppressed in CPT2$^{A-/-}$ gWAT specifically in high-fat-fed conditions (Figure 7A). Therefore, CPT2$^{A-/-}$ gWAT gene expression was consistent with greater ROS detoxification and lower ROS generation. This led us to look at the mRNA abundance of adipokines, cytokines, and inflammatory markers in gWAT of control and CPT2$^{A-/-}$ mice. *Cox2* mRNA abundance, which produces inflammatory mediators, was robustly suppressed in high-fat-fed CPT2$^{A-/-}$ gWAT compared to controls (Figure 7A). *Adiponectin* mRNA abundance, which is regulated by redox and suppressed in diabetes, rebounded in high-fat-fed CPT2$^{A-/-}$ gWAT back to low-fat-fed levels (Figure 7B). Although *Leptin* mRNA abundance in gWAT was unchanged between genotypes, *Fgf-21* and *Adipsin* were significantly suppressed in low-fat-fed CPT2$^{A-/-}$ mice (Figure 7B). Since *Adipsin*, also known as complement factor D, is involved in the inflammatory response, we next looked at inflammatory markers in CPT2$^{A-/-}$ gWAT. Although, the macrophage marker *F4/80* was unchanged between CPT2$^{A-/-}$ and control mice, there was a suppression in *Cd11b* (*Mac-1*), a marker for activated macrophages, in high-fat-fed CPT2$^{A-/-}$ gWAT (Figure 7C). Consistent with these changes, there was a marked suppression in inflammatory gene expression as evidenced by lower mRNA abundance of *Mip-1a* and *Il-1b*, as well as a trend for the suppression in *Mip1b* in high-fat-fed CPT2$^{A-/-}$ gWAT (Figure 7C). Additionally, the mRNA abundance of the anti-inflammatory cytokine *Il-10* was significantly suppressed in high-fat-fed CPT2$^{A-/-}$ gWAT. There were no changes in the mRNA abundance of several important inflammatory and insulin-resistance-promoting cytokines/chemokines *Tnf-α*, *Il-6*, or *Mcp1* in control and CPT2$^{A-/-}$ gWAT (Figure 7C). Finally, we measured oxidized lipids in gWAT and serum of low- and high-fat-fed control and CPT2$^{A-/-}$ mice. The high-fat diet-induced increase in lipid peroxidation observed in control gWAT and serum was repressed in CPT2$^{A-/-}$ mice (Figure 7D). These data show that high-fat feeding requires mitochondrial oxidation to potentiate high-fat diet-induced oxidative stress and inflammation.

Improvements in CPT2$^{A-/-}$ Adipose Tissue Oxidative Stress Did Not Lead to Improved Systemic Glucose Tolerance

Adipose oxidative stress and inflammation induced by high-fat feeding has been suggested to initiate a cascade that leads to systemic insulin resistance (Glass and Olefsky, 2012; Hotamisligil, 2010). Because we have greatly suppressed oxidative stress and improved inflammatory markers in CPT2$^{A-/-}$ mice fed a high-fat diet, we determined glucose tolerance for control and CPT2$^{A-/-}$ mice fed both low- and high-fat diets by glucose and insulin tolerance tests. Consistent with an increase in adiposity, low-fat-fed CPT2$^{A-/-}$ mice exhibited greater glucose intolerance exhibited by impaired glucose disposal during the glucose tolerance test (GTT) and a strong trend toward impaired glucose clearance in response to insulin in the ITT (Figure 7E). These defects in glucose tolerance are not seen in chow-fed mice, suggesting that the high content of simple sugars (i.e., sucrose) promote lipid deposition and glucose intolerance in adipose in the absence of fatty acid oxidation (Figure S5). In contrast, high-fat-fed control and CPT2$^{A-/-}$ mice had similar glucose dynamics (Figure 7F). Therefore, the improvements in adiposity, oxidative stress, and inflammation in high-fat-fed CPT2$^{A-/-}$ mice were not sufficient to reverse systemic insulin resistance and glucose intolerance and are not consistent with a requirement for adipose-derived ROS in mediating systemic glucose intolerance.

DISCUSSION

Obesity is the result of energy imbalance. As caloric intake exceeds expenditure, metabolic flux is directed into energy reserves, primarily as triglyceride in adipose tissue. Conversely, when caloric expenditure exceeds intake, these reserves are mobilized to provide physiological fuel. Alterations in adipocyte-specific metabolism can lead to systemic changes in adiposity, body weight, and glucose tolerance (Abel et al., 2001; Ahmadian et al., 2011; Lodhi et al., 2012; Vernochet et al., 2012). The suppression of adipocyte fatty acid oxidation is often invoked as a mechanism to explain mouse models that are obese in the absence of increased food intake. Although this is not an implausible idea, it has lacked an experimental underpinning. Contrary to this notion, we have shown that the lack of adipocyte long-chain fatty acid oxidation does not lead to changes in body weight under standard laboratory conditions even when challenged by calorically dense diets.

BAT can dramatically increase metabolic rate and dissipate large amounts of stored lipids in a relatively short time once activated. Transgenic mice with increased BAT mass correlate nicely with resistance to weight gain (Harms and Seale, 2013). The transplantation of large amounts of BAT into mice improves their glucose tolerance but does little to improve their body weight (Stanford et al., 2013). This may point to a robust endocrine rather than bioenergetic contribution of BAT. In fact, in the absence of cold-induced activation, the role of brown adipocyte bioenergetics in obesity remains controversial (Kozak, 2010). Similar to CPT2$^{A-/-}$ mice, UCP1KO mice are resistant to, rather than prone to, diet-induced obesity at 20°C (Liu et al., 2003). Aging or a thermoneutral environment can alter this phenotype to produce obese-prone UCP1KO mice (Feldmann et al., 2009; Kontani et al., 2005). Additionally, the loss of ACSL1 in adipocytes, which renders mice unable to efficiently activate fatty

(E) Intraperitoneal glucose tolerance test (ipGTT) and intraperitoneal insulin tolerance test (ipITT) including area under the curve and area above the curve, respectively, for control and CPT2$^{A-/-}$ mice fed a low-fat diet (n = 9).
(F) ipGTT and ipITT including area under the curve and area above the curve, respectively, for control and CPT2$^{A-/-}$ mice fed a high-fat diet (n = 13–18).
Data are expressed as mean ± SEM. **p < 0.005; *p < 0.05.

acids for oxidation, leads to an increase in adiposity with low-fat feeding similar to CPT2$^{A-/-}$ mice (Ellis et al., 2010). Activation of catabolic processes in tissue other than adipose, needed to maintain body temperature, likely accounts for their lack of body-weight change and altered adiposity (Bal et al., 2012). These experiments illuminate a compensatory role of basal metabolic rate to compensate for the loss of BAT mediated thermogenesis; however, little is known about how the basal metabolic rate is regulated, where it emanates from, or mechanistically how it contributes to body temperature or body weight.

The phosphorylation of CREB by adrenergic stimulation induces the robust expression of thermogenic genes in BAT, including *Ucp1* and *Pgc1α*. Conversely, several nuclear hormone receptors and corepressors such as LXRα and RIP140 negatively regulate thermogenic genes (Leonardsson et al., 2004; Wang et al., 2008). LXRα selectively represses *Ucp1* induction by binding adjacent to CREB on the *Ucp1* promoter. The crosstalk between fatty acid metabolism and thermogenic programing is likely mediated by fatty acid metabolites acting as ligands for nuclear hormone receptors to suppress agonist-induced transcriptional control. The fact that ACSL1$^{A-/-}$ mice are cold intolerant but still retain thermogenic gene induction suggests the defect in CPT2$^{A-/-}$ BAT gene expression lies between the activation of fatty acids and their oxidation (Ellis et al., 2010). Similar to CPT2$^{A-/-}$ mice, systemic carnitine deficiency also results in a suppression of *Ucp1* expression in BAT (Ozaki et al., 2011). These data suggest that an accumulation of fatty acid metabolites, such as long chain acyl-CoAs, for example, may be critical nuclear hormone ligands acting as negative metabolic feedback sensors to link metabolic capacity to nuclear encoded mitochondrial gene expression.

Although CPT2$^{A-/-}$ mice were unable to generate heat or oxidize fatty acids in BAT and WAT, they did not have changes in body weight when fed standard chow, low-fat, or high-fat diets. Under low-fat feeding, the mice gained more adiposity, but this was likely due to the high sucrose content in the diet, as chow feeding did not elicit increased adiposity. Low-fat-fed mice have enhanced de novo fatty acid synthesis in WAT, likely in part due to decreased concentrations of cellular L-carnitine and acetylcarnitine. Lower L-carnitine and acetylcarnitine levels can shift mitochondria to increased de novo lipogenesis by the inability to dissipate mitochondrial acetyl-CoA and thereby its allosteric effects on the pyruvate dehydrogenase complex and pyruvate carboxylase (Muoio et al., 2012). High-fat feeding elicited a suppression in adiposity in CPT2$^{A-/-}$ mice and a concomitant ~2-fold increase in circulating ketones. Severe forms of cold intolerance such as ACSL1$^{A-/-}$, CPT2$^{A-/-}$ mice, and UCP1KO mice are either neutral or mildly resistant to high-fat diet-induced obesity at room temperature (Ellis et al., 2010; Liu et al., 2003). However, mouse models with mild cold intolerance are obese prone at room temperature (Liu et al., 2014; Müller et al., 2013). One possible explanation for this paradox is that mild BAT dysfunction may evade the reflexive compensation required to maintain body temperature, resulting in increased weight gain. Long-term housing of mice at thermoneutrality may relieve this compensation and generate obese-prone CPT2$^{A-/-}$ mice similar to UCP1KO mice (Feldmann et al., 2009). It is not clear, however, what the role of uncoupling and heat generation is at thermoneutrality. Is there still a need for BAT thermogenesis, or is uncoupling required for something else entirely, such as the generation of metabolic water (Neess et al., 2013; Nelson et al., 1973)?

It is clear that fatty acid oxidation is important in BAT; however, how does fatty acid oxidation in WAT contribute? The high oxidative stress and inflammation seen after long-term high-fat feeding has been attributed to fatty acid metabolism, which we confirm here (Furukawa et al., 2004). Here, we have evidence that the rate setting step in fatty acid oxidation is transcriptionally upregulated 6-fold in high-fat-fed gWAT (Figure S2A). We also observed increases in oxidative stress and inflammation under a high-fat diet, and these changes are greatly reduced in the absence of adipose fatty acid oxidation. Systemic glucose intolerance attributed to local adipose dysfunction was not, however, ameliorated by the loss of CPT2. We observed a suppression in gWAT inflammation in CPT2$^{A-/-}$ mice, as evidenced by a suppression in *Cd11b*, *Cox2*, *Mip1a*, and *Il1b*. The major and likely most relevant inflammatory mediators for insulin resistance such as *Tnf-α* and *Mcp1*, for example, were unchanged (Hotamisligil, 2010). Therefore, these important mediators of obesity-induced insulin resistance were not dependent on adipose mitochondrial long-chain fatty acid β-oxidation.

In summary, adipose tissue fatty acid oxidation is critical for acute adaptation to the cold by providing both the energy required to fuel heat generation and the transcriptional regulation of BAT thermogenesis. Additionally, white adipose fatty acid oxidation potentiates high-fat diet-induced oxidative stress and inflammation; however, the improvements seen in CPT2$^{A-/-}$ mice were not sufficient to reverse systemic insulin resistance. Taken together, adipose fatty acid oxidation is an important metabolic process for environmental and nutritional homeostasis.

EXPERIMENTAL PROCEDURES

Animals and Diets

CPT2$^{lox/lox}$ mice were generated by targeting *loxP* sequences to introns flanking exon 4 of the mouse *Cpt2* gene by homologous recombination in C57Bl/6 embryonic stem cells by standard methods. To produce mice with a loss of CPT2 specifically in adipocytes, we bred CPT2$^{lox/lox}$ mice to adiponectin-Cre transgenic mice (Eguchi et al., 2011). CPT2$^{A-/-}$ and littermate CPT2$^{lox/lox}$ mice were housed in a facility with ventilated racks on a 14 hr light/10 hr dark cycle with access to a standard chow diet (Etruded Global Rodent Diet, Harlan Laboratories). For the diet study, mice were fed a 10% low-fat (D12450J, Research Diets) or a 60% high-fat diet (D12492, Research Diets) from 6 weeks to 18 weeks of age (12 weeks on diet). At week 10 of the diet, mice were subjected to a glucose tolerance test by intraperitoneal injection of glucose (0.75 g/kg) and measuring tail blood glucose at 0, 15, 30, 60, and 120 min. At week 11 of the diet, insulin tolerance tests were performed via intraperitoneal injection of insulin (0.6 U/kg) and measuring tail blood glucose at 0, 15, 30, 60, and 90 min (Nova Max Plus). Body weights were measured on a weekly basis. For thermogenesis experiments, 12-week-old mice had food withdrawn for 4 hr and placed in a 4°C environment for 3 hr. Body temperature was measured hourly by a rectal probe thermometer (BAT-12, Physitemp). BAT, iWAT, gWAT, liver, and muscle were collected and frozen in liquid nitrogen. Serum was collected from all mice, and free glycerol and TAG (Sigma), β-hydroxybutyrate (StanBio), total cholesterol (Wako), and NEFA (Wako) were measured colorimetrically. BAT collected from thermogenesis experiments was homogenized in Media I (10 mM Tris [pH 8.0], 1 mM EDTA, and 0.25 M

sucrose) to measure TAG (Sigma). For in vivo studies, 20-week-old CPT2$^{A-/-}$ and littermate CPT2$^{lox/lox}$ mice were injected with CL-316243 (10 mg/kg, Santa Cruz) or vehicle. To determine the protein expression of phospho-CREB, CREB, phospho-mTOR and mTOR, CL-316243 (10 mg/kg) or vehicle was injected to 20-week old mice and tissues were collected after 30min. For cold acclimation, 12–14 week old CPT2$^{A-/-}$ and littermate CPT2$^{lox/lox}$ mice were housed in an animal incubator at 18°C on a 12 hr light/12 hr dark cycle with access to a standard chow diet for one week. The incubator was lowered to 15°C the following week. Then mice had food withdrawn for 4 hr and placed in a 4°C environment for 4 hr. For thermoneutral adaptation, 12-week-old CPT2$^{A-/-}$ and littermate CPT2$^{lox/lox}$ mice were housed in an animal incubator at 30°C on a 12 hr light/12 hr dark cycle with access to a standard chow diet for 2 weeks. At 14 weeks of age, the mice were injected with either CL-316243 (10 mg/kg) or vehicle for 3 hr. All procedures were performed in accordance with the NIH's *Guide for the Care and Use of Laboratory Animals* and under the approval of the Johns Hopkins Medical School Animal Care and Use Committee.

Body Composition and Metabolic Analysis

Body fat and lean mass were determined by magnetic resonance imaging (minispec MQ10) in 18-week-old mice. To measure whole-animal energy utilization, 12-week-old male CPT2$^{A-/-}$ and CPT2$^{lox/lox}$ littermates that were fed a standard chow diet were individually housed in Comprehensive Laboratory Animal Monitoring System (Columbus Instruments) cages on a 12 hr light/12 hr dark cycle. O_2 and CO_2 consumption and production, respectively, food and water intake, and home-cage activity were measured continuously. After a 2-day acclimation period, data were collected for 48 hr for ad libitum and a 24 hr fasting period. At the end of the study, the same mice were injected with CL-316243 (10 mg/kg) and were monitored for 3 hr.

In Vivo Acetate Incorporation Experiment

Six-week-old CPT2$^{A-/-}$ and littermate CPT2$^{lox/lox}$ mice were fed a 10% low-fat diet for 2 weeks. At 8 weeks of age, mice were injected with 10 μCi of [^{3}H] acetate for 3 hr. BAT, gWAT, and liver were collected, and lipid was extracted using the Folch method. Aliquots of the samples were counted for [^{3}H] labeled lipids. All samples were counted using the Beckman Coulter scintillation counter (LS 6000SC, Beckman Coulter).

Cell Culture

CPT2$^{lox/lox}$ primary MEFs were derived from embryos and cultured in Dulbecco's modified Eagle's medium (DMEM) supplemented with 10% fetal bovine serum (FBS) and 1% penicillin/streptomycin. To generate CPT2$^{lox/lox}$ and CPT2KO MEFs, cells were first transduced with large T antigen-expressing lentiviral particles (LVP016-Neo, GenTarget) for 48 hr and G418 (300 μg/mL) was added to select for positive cells. The selected cells were then transduced with red fluorescent protein (LVP023, GenTarget) or CRE-2A-RFP (LVP013, GenTarget) lentiviral particles and selected with blasticidin (10 μg/mL) to generate CPT2$^{lox/lox}$ and CPT2KO MEFs, respectively.

MEFs were plated in T25 flasks at 70% confluency and incubated in DMEM supplemented with 10% FBS and 1% penicillin/streptomycin overnight. The cells were washed with 1× PBS and the reaction mixture for [U-^{14}C] glucose (DMEM [A14430-01], 2 mM glutamine, 2.5 mM glucose, 0.5 mM sodium pyruvate, 0.1 μCi of [U-^{14}C] glucose) or [2-^{14}C] pyruvate (DMEM [A14430-01], 2 mM glutamine, 2.5 mM glucose, 0.5 mM sodium pyruvate, 0.1 μCi of [2-^{14}C] pyruvate) was added to cells. The flasks were sealed with a rubber stopper containing a hanging well filled with filter paper and incubated in a 37°C incubator for 4 hr. Carbon dioxide was trapped by adding 150 μl of 1 M NaOH to the filter paper in the center well and 200 μl of 1 M perchloric acid to the reaction mixture. Then the samples were incubated at 55°C for 1 hr and the filter paper was placed in scintillation fluid and counted. For [1-^{14}C] oleate oxidation, the reaction mixture (DMEM supplemented with 0.1 μCi of [1-^{14}C] oleate, 100 μM L-carnitine hydrochloride [Sigma], and 0.2% BSA) or the reaction mixture containing 100 μM etomoxir was added to cells and incubated in a 37°C incubator for 4 hr. Carbon dioxide was collected and counted as described above. For [1-^{14}C] lignoceric acid oxidation, the reaction mixture (DMEM supplemented with 0.1 μCi of [1-^{14}C] lignocerate and 0.2% BSA) was added to cells and incubated overnight in a 37°C incubator. Carbon dioxide was collected and counted as described above.

For substrate flux into lipids, MEFs were plated in 24-well plates and incubated in DMEM supplemented with 10% FBS and 1% penicillin/streptomycin overnight and washed with 1× PBS the next day. The cells were incubated in [2-^{14}C] pyruvate (DMEM [A14430-01], 2 mM glutamine, 2.5 mM glucose, 0.5 mM sodium pyruvate, 0.1 μCi of [2-^{14}C] pyruvate) or [^{3}H] acetate (DMEM supplemented with 0.3 μCi [^{3}H] acetate) reaction mixture and incubated at 37°C for 4 hr. Lipid was extracted using the Folch method, and aliquots of the samples were counted for [^{3}H]-labeled lipids.

Adipose Tissue Oxidation Experiments

BAT, iWAT, and gWAT were collected from 20-week-old CPT2$^{A-/-}$ and littermate CPT2$^{lox/lox}$ male mice and placed in an incubation chamber containing the reaction mixture (DMEM supplemented with 0.1 μCi of [1-^{14}C] oleate, 100 μM L-carnitine (Sigma), and 0.2% BSA). The chamber contained a center well filled with filter paper and sealed with a rubber stopper. The incubation chambers were in a 37°C shaking water bath for 4 hr. Trapping carbon dioxide was collected as described above. In vivo fatty acid oxidation was carried out as previously described (Reamy and Wolfgang, 2011; Rodriguez and Wolfgang, 2012).

BAT Explant Experiments

BAT was collected from 20-week-old mice. Each BAT nugget was cut in half and placed in media (DMEM, 10% FBS, 200 μM total of palmitate and oleate at a 1:2 molar ratio, BSA at a 1:3 molar ratio with total fatty acids). Forskolin (10 μM, Sigma), isoproterenol (10 μM, Sigma), or CL-316243 (10 μM, Santa Cruz) was added to tubes and incubated in a 37°C water bath for 3 hr. The tissues were frozen in liquid nitrogen for further analysis.

Analysis of Gene Expression and Mitochondrial DNA by Quantitative PCR

Total RNA was isolated using the RNeasy Mini Kit (QIAGEN). A total of 1–2 μg of RNA was reverse transcribed using the High Capacity cDNA Reverse Transcription Kit (Applied Biosciences). The cDNA was diluted to 2 ng/μL and was amplified by specific primers in a 20 μl reaction using SsoAdvanced SYBR Green Supermix (Bio-Rad). WAT cDNA from CPT2$^{A-/-}$ and littermate CPT2$^{lox/lox}$ mice on a high-fat diet was prepared according to the manufacturer's protocol for the mouse oxidative stress PCR array (SA Biosciences). Analysis of gene expression was carried out in a CFX Connect Real-Time System (Bio-Rad). For each gene, mRNA expression was calculated as 2^deltaCT relative to cyclophilin A expression. For mitochondrial DNA analysis, total DNA was prepared using the QIAmp DNA mini Kit (QIAGEN). Mitochondrial DNA was amplified using primers Co1 and Nd1 and was normalized to genomic DNA by primers amplifying H19 from genomic DNA as previously described (Ellis et al., 2011). Primers and gene information are provided in Table S1.

Western Blot Analysis

BAT collected after acute CL-316243 or vehicle injection was homogenized in 1× RIPA buffer with protease inhibitors (Complete Mini, Roche) and phosphatase inhibitors (PhosSTOP, Roche). All other tissues from the diet study were homogenized in 1× RIPA buffer with protease inhibitors (Complete Mini, Roche). BAT, gWAT, iWAT, and liver samples from thermogenesis experiments were homogenized in Media I with protease inhibitors. All samples were spun down at 10,000 rpm for 20 min, and supernatant was collected and assayed by the Pierce BCA Protein Assay Kit (Thermo Scientific) to determine the concentration of protein. A total of 30 μg of protein was subjected to SDS-PAGE and transferred to a nitrocellulose membrane (Protran BA 83, Whatman). The blots were probed with the following antibodies: Uqcrc2 (mitoprofile Total OXPHOS, Abcam), Sdhb (mitoprofile Total OXPHOS, Abcam), Acsf3 (Pierce), phospho-CREB (Ser-133, Millipore), CREB (Pierce), phospho-mTOR (Cell Signaling), and mTOR (Cell Signaling) using the appropriate secondary antibodies conjugated to horseradish peroxidase. Fasn (BD Biosciences), Aco2 (Cell Signaling), Mcad (GeneTex), Hsc70 (Santa Cruz), Sod2, and Hadha (GeneTex) used the appropriate Cy5 (Life Technologies) or Cy3 (Life Technologies) fluorescent secondary antibodies.

Oxidative Damage

Thiobarbituric acid reactive substances (TBARS) were determined in gWAT, and serum from 20-week-old male CPT2$^{A-/-}$ and littermate CPT2$^{lox/lox}$ mice fed a high- or low-fat diet. WAT was prepared by homogenizing 100 mg of tissue in 500 μl of 1× RIPA buffer with protease inhibitors (Complete Mini, Roche). Homogenates were centrifuged at 1,600 × *g* for 10 min, and 25 μl of supernatant was used to determine oxidative damage via the TBARS Assay Kit (Cayman Chemical Company).

Acylcarnitine Analysis

iWAT from CPT2$^{A-/-}$ and littermate CPT2$^{lox/lox}$ mice were collected and frozen in liquid nitrogen. Approximately 100 mg of tissue was analyzed for acylcarnitine content at the University of Michigan Metabolomics Core Services.

Statistical Analysis

When only two genotypes were analyzed, statistical significance was determined using a student's t test. Two-way ANOVA was utilized for repeated-measures such as body temperature over time, weight gain over time, GTT, and insulin tolerance test. Significance was determined for p values < 0.05.

SUPPLEMENTAL INFORMATION

Supplemental Information includes five figures and one table and can be found with this article online at http://dx.doi.org/10.1016/j.celrep.2014.12.023.

AUTHOR CONTRIBUTIONS

J.L., J.M.E., and M.J.W. performed experiments and wrote the manuscript.

ACKNOWLEDGMENTS

The authors would like to thank Susan Aja for assistance with the metabolic cage studies, Natasha Zachara for reagents, and G. W. Wong for helpful discussions. This work was supported in part by a NIH grant R01NS072241 to M.J.W. This work utilized Metabolomics Core Services supported by grant U24 DK097153 of NIH Common Funds Project to the University of Michigan.

Received: June 23, 2014
Revised: November 4, 2014
Accepted: December 11, 2014
Published: January 8, 2015

REFERENCES

Abel, E.D., Peroni, O., Kim, J.K., Kim, Y.B., Boss, O., Hadro, E., Minnemann, T., Shulman, G.I., and Kahn, B.B. (2001). Adipose-selective targeting of the GLUT4 gene impairs insulin action in muscle and liver. Nature *409*, 729–733.

Abu-Elheiga, L., Matzuk, M.M., Abo-Hashema, K.A., and Wakil, S.J. (2001). Continuous fatty acid oxidation and reduced fat storage in mice lacking acetyl-CoA carboxylase 2. Science *291*, 2613–2616.

Ahmadian, M., Abbott, M.J., Tang, T., Hudak, C.S., Kim, Y., Bruss, M., Hellerstein, M.K., Lee, H.Y., Samuel, V.T., Shulman, G.I., et al. (2011). Desnutrin/ATGL is regulated by AMPK and is required for a brown adipose phenotype. Cell Metab. *13*, 739–748.

Bal, N.C., Maurya, S.K., Sopariwala, D.H., Sahoo, S.K., Gupta, S.C., Shaikh, S.A., Pant, M., Rowland, L.A., Bombardier, E., Goonasekera, S.A., et al. (2012). Sarcolipin is a newly identified regulator of muscle-based thermogenesis in mammals. Nat. Med. *18*, 1575–1579.

Eguchi, J., Wang, X., Yu, S., Kershaw, E.E., Chiu, P.C., Dushay, J., Estall, J.L., Klein, U., Maratos-Flier, E., and Rosen, E.D. (2011). Transcriptional control of adipose lipid handling by IRF4. Cell Metab. *13*, 249–259.

Ellis, J.M., Li, L.O., Wu, P.C., Koves, T.R., Ilkayeva, O., Stevens, R.D., Watkins, S.M., Muoio, D.M., and Coleman, R.A. (2010). Adipose acyl-CoA synthetase-1 directs fatty acids toward beta-oxidation and is required for cold thermogenesis. Cell Metab. *12*, 53–64.

Ellis, J.M., Mentock, S.M., Depetrillo, M.A., Koves, T.R., Sen, S., Watkins, S.M., Muoio, D.M., Cline, G.W., Taegtmeyer, H., Shulman, G.I., et al. (2011). Mouse cardiac acyl coenzyme a synthetase 1 deficiency impairs Fatty Acid oxidation and induces cardiac hypertrophy. Mol. Cell. Biol. *31*, 1252–1262.

Feldmann, H.M., Golozoubova, V., Cannon, B., and Nedergaard, J. (2009). UCP1 ablation induces obesity and abolishes diet-induced thermogenesis in mice exempt from thermal stress by living at thermoneutrality. Cell Metab. *9*, 203–209.

Furukawa, S., Fujita, T., Shimabukuro, M., Iwaki, M., Yamada, Y., Nakajima, Y., Nakayama, O., Makishima, M., Matsuda, M., and Shimomura, I. (2004). Increased oxidative stress in obesity and its impact on metabolic syndrome. J. Clin. Invest. *114*, 1752–1761.

Glass, C.K., and Olefsky, J.M. (2012). Inflammation and lipid signaling in the etiology of insulin resistance. Cell Metab. *15*, 635–645.

Golozoubova, V., Hohtola, E., Matthias, A., Jacobsson, A., Cannon, B., and Nedergaard, J. (2001). Only UCP1 can mediate adaptive nonshivering thermogenesis in the cold. FASEB J. *15*, 2048–2050.

Guerra, C., Koza, R.A., Walsh, K., Kurtz, D.M., Wood, P.A., and Kozak, L.P. (1998). Abnormal nonshivering thermogenesis in mice with inherited defects of fatty acid oxidation. J. Clin. Invest. *102*, 1724–1731.

Harms, M., and Seale, P. (2013). Brown and beige fat: development, function and therapeutic potential. Nat. Med. *19*, 1252–1263.

Haynie, K.R., Vandanmagsar, B., Wicks, S.E., Zhang, J., and Mynatt, R.L. (2014). Inhibition of carnitine palymitoyltransferase1b induces cardiac hypertrophy and mortality in mice. Diabetes Obes. Metab. *16*, 757–760.

Hotamisligil, G.S. (2010). Endoplasmic reticulum stress and the inflammatory basis of metabolic disease. Cell *140*, 900–917.

Houstis, N., Rosen, E.D., and Lander, E.S. (2006). Reactive oxygen species have a causal role in multiple forms of insulin resistance. Nature *440*, 944–948.

Hsiao, Y.S., Jogl, G., Esser, V., and Tong, L. (2006). Crystal structure of rat carnitine palmitoyltransferase II (CPT-II). Biochem. Biophys. Res. Commun. *346*, 974–980.

Ji, S., You, Y., Kerner, J., Hoppel, C.L., Schoeb, T.R., Chick, W.S., Hamm, D.A., Sharer, J.D., and Wood, P.A. (2008). Homozygous carnitine palmitoyltransferase 1b (muscle isoform) deficiency is lethal in the mouse. Mol. Genet. Metab. *93*, 314–322.

Keaney, J.F., Jr., Larson, M.G., Vasan, R.S., Wilson, P.W., Lipinska, I., Corey, D., Massaro, J.M., Sutherland, P., Vita, J.A., and Benjamin, E.J.; Framingham Study (2003). Obesity and systemic oxidative stress: clinical correlates of oxidative stress in the Framingham Study. Arterioscler. Thromb. Vasc. Biol. *23*, 434–439.

Kontani, Y., Wang, Y., Kimura, K., Inokuma, K.I., Saito, M., Suzuki-Miura, T., Wang, Z., Sato, Y., Mori, N., and Yamashita, H. (2005). UCP1 deficiency increases susceptibility to diet-induced obesity with age. Aging Cell *4*, 147–155.

Kozak, L.P. (2010). Brown fat and the myth of diet-induced thermogenesis. Cell Metab. *11*, 263–267.

Kusminski, C.M., and Scherer, P.E. (2012). Mitochondrial dysfunction in white adipose tissue. Trends Endocrinol. Metab. *23*, 435–443.

Leonardsson, G., Steel, J.H., Christian, M., Pocock, V., Milligan, S., Bell, J., So, P.W., Medina-Gomez, G., Vidal-Puig, A., White, R., and Parker, M.G. (2004). Nuclear receptor corepressor RIP140 regulates fat accumulation. Proc. Natl. Acad. Sci. USA *101*, 8437–8442.

Liu, X., Rossmeisl, M., McClaine, J., Riachi, M., Harper, M.E., and Kozak, L.P. (2003). Paradoxical resistance to diet-induced obesity in UCP1-deficient mice. J. Clin. Invest. *111*, 399–407.

Liu, M., Bai, J., He, S., Villarreal, R., Hu, D., Zhang, C., Yang, X., Liang, H., Slaga, T.J., Yu, Y., et al. (2014). Grb10 promotes lipolysis and thermogenesis by phosphorylation-dependent feedback inhibition of mTORC1. Cell Metab. *19*, 967–980.

Lodhi, I.J., Yin, L., Jensen-Urstad, A.P., Funai, K., Coleman, T., Baird, J.H., El Ramahi, M.K., Razani, B., Song, H., Fu-Hsu, F., et al. (2012). Inhibiting adipose tissue lipogenesis reprograms thermogenesis and PPARγ activation to decrease diet-induced obesity. Cell Metab. *16*, 189–201.

Longo, N., Amat di San Filippo, C., and Pasquali, M. (2006). Disorders of carnitine transport and the carnitine cycle. Am. J. Med. Genet. C. Semin. Med. Genet. *142C*, 77–85.

Lowell, B.B., S-Susulic, V., Hamann, A., Lawitts, J.A., Himms-Hagen, J., Boyer, B.B., Kozak, L.P., and Flier, J.S. (1993). Development of obesity in transgenic mice after genetic ablation of brown adipose tissue. Nature *366*, 740–742.

Müller, T.D., Lee, S.J., Jastroch, M., Kabra, D., Stemmer, K., Aichler, M., Abplanalp, B., Ananthakrishnan, G., Bhardwaj, N., Collins, S., et al. (2013). p62 links β-adrenergic input to mitochondrial function and thermogenesis. J. Clin. Invest. *123*, 469–478.

Muoio, D.M., Noland, R.C., Kovalik, J.P., Seiler, S.E., Davies, M.N., DeBalsi, K.L., Ilkayeva, O.R., Stevens, R.D., Kheterpal, I., Zhang, J., et al. (2012). Muscle-specific deletion of carnitine acetyltransferase compromises glucose tolerance and metabolic flexibility. Cell Metab. *15*, 764–777.

Neess, D., Bek, S., Bloksgaard, M., Marcher, A.B., Færgeman, N.J., and Mandrup, S. (2013). Delayed hepatic adaptation to weaning in ACBP-/- mice is caused by disruption of the epidermal barrier. Cell Rep. *5*, 1403–1412.

Nelson, R.A., Wahner, H.W., Jones, J.D., Ellefson, R.D., and Zollman, P.E. (1973). Metabolism of bears before, during, and after winter sleep. Am. J. Physiol. *224*, 491–496.

Nyman, L.R., Cox, K.B., Hoppel, C.L., Kerner, J., Barnoski, B.L., Hamm, D.A., Tian, L., Schoeb, T.R., and Wood, P.A. (2005). Homozygous carnitine palmitoyltransferase 1a (liver isoform) deficiency is lethal in the mouse. Mol. Genet. Metab. *86*, 179–187.

Ozaki, K., Sano, T., Tsuji, N., Matsuura, T., and Narama, I. (2011). Carnitine is necessary to maintain the phenotype and function of brown adipose tissue. Lab. Invest. *91*, 704–710.

Reamy, A.A., and Wolfgang, M.J. (2011). Carnitine palmitoyltransferase-1c gain-of-function in the brain results in postnatal microencephaly. J. Neurochem. *118*, 388–398.

Rodriguez, S., and Wolfgang, M.J. (2012). Targeted chemical-genetic regulation of protein stability in vivo. Chem. Biol. *19*, 391–398.

Schuler, A.M., Gower, B.A., Matern, D., Rinaldo, P., Vockley, J., and Wood, P.A. (2005). Synergistic heterozygosity in mice with inherited enzyme deficiencies of mitochondrial fatty acid beta-oxidation. Mol. Genet. Metab. *85*, 7–11.

Stanford, K.I., Middelbeek, R.J., Townsend, K.L., An, D., Nygaard, E.B., Hitchcox, K.M., Markan, K.R., Nakano, K., Hirshman, M.F., Tseng, Y.H., and Goodyear, L.J. (2013). Brown adipose tissue regulates glucose homeostasis and insulin sensitivity. J. Clin. Invest. *123*, 215–223.

Tolwani, R.J., Hamm, D.A., Tian, L., Sharer, J.D., Vockley, J., Rinaldo, P., Matern, D., Schoeb, T.R., and Wood, P.A. (2005). Medium-chain acyl-CoA dehydrogenase deficiency in gene-targeted mice. PLoS Genet. *1*, e23.

Tseng, Y.H., Cypess, A.M., and Kahn, C.R. (2010). Cellular bioenergetics as a target for obesity therapy. Nat. Rev. Drug Discov. *9*, 465–482.

Ukropec, J., Anunciado, R.P., Ravussin, Y., Hulver, M.W., and Kozak, L.P. (2006). UCP1-independent thermogenesis in white adipose tissue of cold-acclimated Ucp1-/- mice. J. Biol. Chem. *281*, 31894–31908.

Vernochet, C., Mourier, A., Bezy, O., Macotela, Y., Boucher, J., Rardin, M.J., An, D., Lee, K.Y., Ilkayeva, O.R., Zingaretti, C.M., et al. (2012). Adipose-specific deletion of TFAM increases mitochondrial oxidation and protects mice against obesity and insulin resistance. Cell Metab. *16*, 765–776.

Wang, T., Zang, Y., Ling, W., Corkey, B.E., and Guo, W. (2003). Metabolic partitioning of endogenous fatty acid in adipocytes. Obes. Res. *11*, 880–887.

Wang, H., Zhang, Y., Yehuda-Shnaidman, E., Medvedev, A.V., Kumar, N., Daniel, K.W., Robidoux, J., Czech, M.P., Mangelsdorf, D.J., and Collins, S. (2008). Liver X receptor alpha is a transcriptional repressor of the uncoupling protein 1 gene and the brown fat phenotype. Mol. Cell. Biol. *28*, 2187–2200.

Wolfgang, M.J., and Lane, M.D. (2006). Control of energy homeostasis: role of enzymes and intermediates of fatty acid metabolism in the central nervous system. Annu. Rev. Nutr. *26*, 23–44.